Nanoscale Advances

ROYAL SOCIETY OF CHEMISTRY

COMMUNICATION

View Article Online
View Journal | View Issue

Cite this: *Nanoscale Adv.*, 2020, **2**, 3809

Received 29th June 2020
Accepted 10th July 2020

DOI: 10.1039/d0na00540a

rsc.li/nanoscale-advances

The quantum dot-FRET-based detection of vitamin B12 at a picomolar level†

Sabyasachi Pramanik, *[a] Shilaj Roy[b] and Satyapriya Bhandari *[c]

Herein we report the picomolar level detection of vitamin B12 (VB12) using orange-red emitting ligand-free Mn^{2+}-doped ZnS quantum dots (QDs; $\lambda_{em} = 587$ nm) in an aqueous dispersion. Sensing was achieved following the quenching of the luminescence of the Mn^{2+}-doped ZnS QDs with an increasing concentration of VB12. The Stern–Volmer constant was determined to be 5.2×10^{10} M^{-1}. Importantly, the Mn^{2+}-doped ZnS QDs exhibited high sensitivity towards VB12, with a limit of detection as low as 1.15 ± 0.06 pM (in the linear range of 4.9–29.4 pM) and high selectivity in the presence of interfering amino acids, metal ions, and proteins. Notably, a Förster resonance energy transfer (FRET) mechanism was primarily proposed for the observed quenching of luminescence of Mn^{2+}-doped ZnS QDs upon the addition of VB12. The Förster distance (R_o) and energy transfer efficiency (E) were calculated to be 2.33 nm and 79.3%, respectively. Moreover, the presented QD-FRET-based detection may bring about new avenues for future biosensing applications.

Vitamin B12 (VB12), a well-known micronutrient, is endowed with essential biological roles in the metabolism of cells and maintenance of the nervous system and thus for the protection of human health.[1–16] Deficiency in the level of VB12 may cause cognitive decline in older humans, metabolic abnormalities, anaemia, psychosis and heart disease, while the consumption of additional VB12 can lead to unexpected adverse effects of toxicity and deficiency of folic acid.[1–16] Notably, a country-wide study of the physiological reference range and level of VB12 shows that the reference range was 200–900 pg mL^{-1}, with the limit of the lowest level being 300 pg mL^{-1} (at present), which may indicate a deficiency in VB12 and thus the aforementioned diseases, as in earlier reports.[5] Thus, accurate analytical measurement of VB12, especially at a picomolar level, is of paramount interest in practical clinical diagnosis. Current classical techniques for detecting and measuring VB12 mostly rely on microbiological and chemical techniques.[5] Traditional approaches, such as high-performance liquid chromatography, capillary electrophoresis, mass spectrometry, atomic absorption spectrometry, Raman spectroscopy and UV-vis spectroscopy, have demonstrated their usefulness for the detection of VB12.[1–16] However, these methods have drawbacks associated with high equipment costs, time-consuming measurement, complexity in sample preparation and ultra-trace sensitivity issues.[1–16] On the other hand, fluorometric detection stands out as an alternative method for the sensitive detection of VB12 due to its ease of sample preparation, and uncomplicated and rapid measurement.[6–16] In this regard, several fluorescent organic dyes, proteins, carbon-based quantum dots (C-dots), graphene-modified nanostructures, metallic nanoclusters and Cd-based quantum dots (QDs) have been used to detect VB12.[6–16] For example, (i) a combination of graphene self-assembled multilayers (SAMs) and C-dots have demonstrated their usefulness for the detection of VB12, with a limit of detection (LOD) of 2.58 nM; (ii) the *Bombyx mori* silk fibroin fluorescent protein was used to detect VB12, with a LOD of 20 nM; (iii) CdTe QDs were used to sense VB12 with a LOD of 11 nM and (iv) Cu nanoclusters have demonstrated their usefulness as a nanoprobe for the detection of VB12 with a LOD of 3.3 nM.[6,7,15,16] In addition, various C-dots (either in their bare form or doped with nitrogen or sulfur) showed their usefulness as fluorescent nanoprobes for the detection of VB12, with a LOD as low as 210 pM, up to now.[14] However, the multiple syntheses and critical purification steps for C-dots and nanoclusters have limited their real-life application while toxicity issues related to fluorescent organic dyes and Cd-based QDs have restricted their usage.[6–16] Importantly, the picomolar level detection of VB12, with the help of biocompatible luminescent metal-based QDs, has not yet been explored so far. Hence it is imperative to construct a new, low-cost and biocompatible

[a]*Department of Chemistry, National Institute of Technology Sikkim, Sikkim-737139, India. E-mail: sabyasachi@nitsikkim.ac.in*

[b]*Centre for Nanotechnology, Indian Institute of Technology Guwahati, Assam-781039, India*

[c]*Physics Discipline, Indian Institute of Technology Gandhinagar, Gujrat-382355, India. E-mail: satyapriya.b@iitgn.ac.in*

† Electronic supplementary information (ESI) available: The experimental section, Fig. S1–S6 and Table S1. See DOI: 10.1039/d0na00540a

metal QD-based fluorescent nanoprobe for the picomolar level detection of VB12.

Environmentally sustainable metal-based QDs, especially Mn^{2+}-doped ZnS QDs, have demonstrated their usefulness in bioimaging, white light generation, light emitting devices and optical sensing due to their long-wavelength atomic orange-red emission, photostable nature and lower toxicity.[17–23] For example, (i) white light generation could be possible from Mn^{2+}-doped ZnS QDs followed by complexing their surface with two luminescent inorganic complexes, (ii) a reversible pH nanoprobe (in the physiological range 6.5–10.6) can be fabricated by complexing the surface of Mn^{2+}-doped ZnS QDs with external chelating ligands, (iii) a white light emitting hydrogel, with the capability of enzyme packaging, could also be fabricated followed by engineering of the surface of Mn^{2+}-doped ZnS QDs with ionic liquids.[19–21] Thus, the biocompatibility, ease of aqueous-based fabrication and lower toxicity of Mn^{2+}-doped ZnS QDs make them a prime choice for the luminescence-based sensitive and selective detection of VB12. Until now, there has been no report on the use of Mn^{2+}-doped ZnS QDs as a nanoprobe for the detection of VB12. Thus it is important to show the applicability of Mn^{2+}-doped ZnS QDs as a sensing platform for the detection of VB12.

Remarkably, there are very few reports concerning the Förster resonance energy transfer (FRET)-based sensitive detection of VB12.[6–16] FRET is a non-radiative process where the excitation energy is transferred from donor to acceptor *via* long-range dipole–dipole interaction.[24–26] FRET depends upon factors such as the non-zero integral of spectral overlap between the emission spectrum of the donor and the absorption spectrum of the acceptor, distance (smaller than 10 nm) and relative orientation between donor and acceptor, quantum efficiency of the donor and exclusion of the direct extinction of the acceptor.[24–26] According to earlier reports, metal chalcogenide QDs have demonstrated their usefulness as an efficient donor in various FRET systems but there are few reports concerning the activity of VB12 as an acceptor in a FRET pair.[6–16,24–26] Therefore, it would be significant to use biocompatible Mn^{2+}-doped ZnS QDs as a donor with the accepting ability of VB12 in a FRET pair and demonstrating their use for rapid, sensitive and selective detection of VB12, especially at a picomolar level.

Herein we report the use of orange-red emitting ligand-free Mn^{2+}-doped ZnS QDs ($\lambda_{em} = 587$ nm) for the detection of VB12 at a picomolar level. The quenching of the luminescence of the QDs, with an increasing concentration of VB12, was used to demonstrate the detection of VB12. The Stern–Volmer constant was estimated to be 5.2×10^{10} M^{-1}. Notably, the QDs showed a LOD as low as 1.15 ± 0.06 pM (in the linear range of 4.9–29.4 pM) for VB12. In addition, the QDs displayed high selectivity towards VB12 in the presence of interfering amino acids (such as tryptophan, lysine, arginine, and glycine), metal ions (such as Mg^{2+}, Ca^{2+}, K^{+}, and Na^{+}), and protein (such as bovine serum albumin). The FRET mechanism was primarily proposed for the QD-based detection of VB12. The QDs and VB12 acted as donor and acceptor in the FRET pair. The Förster distance (R_0) and the energy transfer efficiency (E) were estimated to be 2.33 nm and 79.3%, respectively. Up to now, the presented nanoprobe has shown the lowest LOD for the detection of VB12, using environmentally sustainable, low-cost and photostable QDs, in comparison to earlier reported luminescent probes.[6–16]

The details of the fabrication of ligand-free Mn^{2+}-doped ZnS QDs and the technique of sensing of VB12 are described in the ESI.†[19] The as-fabricated Mn^{2+}-doped ZnS QDs exhibited an absorption edge at 310 nm and an intense emission peak at 587 nm (due to the $^4T_1$–$^6A_1$ electronic transition of the Mn^{2+} dopant ions present in the ZnS host)[17–23] at an excitation wavelength of 320 nm (Fig. 1A and B). It should be noted here that the optical emission of Mn^{2+}-doped ZnS QDs is independent of their size and dependent on the population of Mn^{2+} and surface passivation.[17–23] When the emission maxima were probed at 587 nm, the excitation spectrum of Mn^{2+}-doped ZnS QDs appeared at around 320 nm (Fig. S1, ESI†). The average particle size of Mn^{2+}-doped ZnS QDs was estimated to be 4.0 ± 0.6 nm in the transmission electron microscopic (TEM) image analysis (Fig. 1C and D). The selected area electron diffraction (SAED) pattern indicated the crystalline nature of the Mn^{2+}-doped ZnS QDs (inset Fig. 1C). The presence of the 0.3 nm lattice fringe of the (111) plane of cubic ZnS in the high-resolution TEM supported the formation of Mn^{2+}-doped ZnS QDs (Fig. 1E).[19–21] The obtained characteristics peaks of the (111), (220) and (311) lattice planes of cubic ZnS in the powder X-ray diffraction pattern of Mn^{2+}-doped ZnS QDs also supported their successful formation (Fig. 1F).[19–21] Thus, the presented results clearly demonstrated the formation of orange-emitting water-soluble Mn^{2+}-doped ZnS QDs. Additionally, the water dispersion of Mn^{2+}-doped ZnS QDs (with a quantum yield of 0.07 with regard to quinine sulfate as a reference) was found to be stable with regard to their luminescence (at 587 nm) for 48 hours (Fig. S2 and Table S1, ESI†). This indicated the stability of the aqueous dispersion of Mn^{2+}-doped ZnS QDs and thus putting forward their applicability in sensing applications.

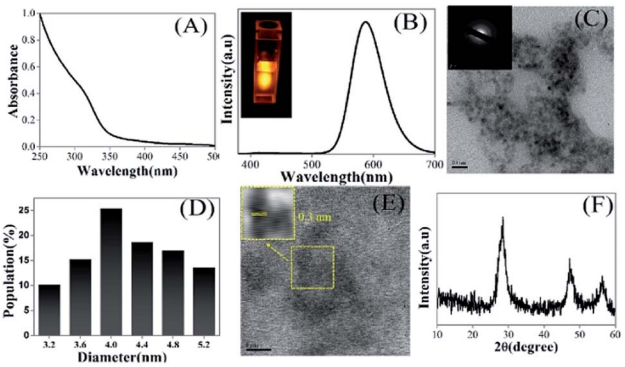

Fig. 1 (A) UV-vis spectrum, (B) emission spectrum ($\lambda_{ex} = 320$ nm; inset: a digital photograph taken using 320 nm light under a spectrofluorometer), (C) a transmission electron microscopy (TEM) image (scale bar = 20 nm) and selected area electron diffraction (SAED) pattern (inset), (D) the particle size distribution, (E) a high-resolution TEM image (scale bar = 5 nm) and corresponding inverse fast Fourier transformed image (inset), and (F) the powder X-ray diffraction (XRD) pattern of ligand-free Mn^{2+}-doped ZnS QDs.

Upon sequential addition of VB12, the steady decrease in the emission intensity (at 587 nm) of Mn^{2+}-doped ZnS QDs (with absorbance of 0.3 at 320 nm) was noted (Fig. 2A). This enhanced quenching of the luminescence of Mn^{2+}-doped ZnS QDs prompted by the presence of an increasing concentration of VB12 indicates that Mn^{2+}-doped ZnS QDs can be used for the detection of VB12 in the range of 4.9–54.1 pM. Notably, quenching in emission intensity of Mn^{2+}-doped ZnS QDs (close to 80%) was observed up to a concentration of 49.2 pM of VB12 (Fig. 2B). While no significant changes with regard to the quenching of emission intensity of Mn^{2+}-doped ZnS QDs, following the addition of a higher amount (>49.2 pM) of VB12, was noticed. Similar observation of quenching was made in terms of the excitation spectrum of Mn^{2+}-doped ZnS QDs when VB12 was added (Fig. S1, ESI†). Accordingly, a linear relationship (with correlation coefficient 0.96) between the change in the luminescence intensity (ΔI_{587}) of Mn^{2+}-doped ZnS QDs and concentration of VB12 (in the range 4.9–29.4 pM) was observed (Fig. 2C). The LOD was estimated by using the $3\sigma/K$ relation; where σ represents the standard deviation of the luminescence intensity of the Mn^{2+}-doped ZnS QDs at 587 nm and K signifies the slope obtained from a plot of the change in the emission intensity of Mn^{2+}-doped ZnS QDs against the increasing concentration of VB12. The LOD of VB12 was estimated to be 1.15 ± 0.06 pM. Until now, this is the most highly sensitive detection of VB12, especially at a picomolar level, compared to earlier reported luminescent nanoprobes (Table 1).[6–16] Hence, the current Mn^{2+}-doped ZnS QDs could be able to detect a trace

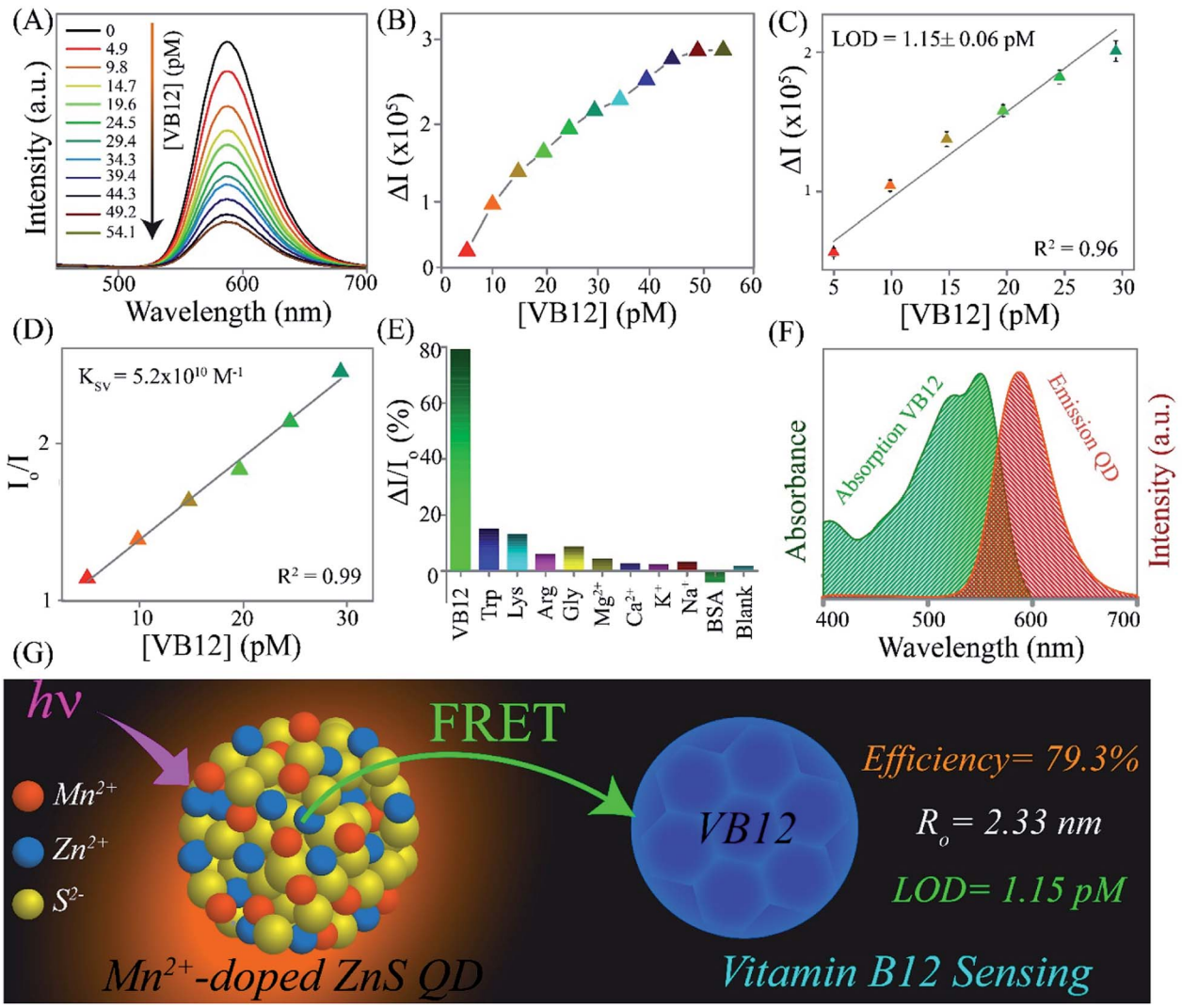

Fig. 2 (A) Emission spectra (λ_{ex} = 320 nm) and (B) changes in the luminescence intensity (ΔI_{587}) of Mn^{2+}-doped ZnS QDs (with an absorbance of 0.3 at 320 nm) following the sequential addition of different concentrations of VB12 in the range 4.9–54.1 pM. (C) Linearity between ΔI_{587} and concentration of VB12 in the range 4.9–29.4 pM. This experiment was performed in triplicate. (D) Stern–Volmer plot of the changes in intensity ratio (I_o/I) of Mn^{2+}-doped ZnS QDs against the concentration of VB12 in the range 4.9–29.4 pM. (E) Comparison of the luminescence intensity ratio (%) of Mn^{2+}-doped ZnS QDs followed by the addition of higher amounts (at a μM scale) of interfering amino acids (such as Trp, Lys, Arg, and Gly), metal ions (such as Mg^{2+}, Ca^{2+}, K^+, and Na^+), and proteins (such as BSA). The concentration of interfering substances used is 3.2 μM, while a 49.2 pM concentration was used for VB12. (F) The spectral overlap between the UV-vis spectrum of VB_{12} and emission spectrum (λ_{ex} = 320 nm) of Mn^{2+}-doped ZnS QDs. (G) A schematic illustration of the mechanism of VB12 FRET-based sensing by Mn^{2+}-doped ZnS QDs.

Table 1 A comparison of various luminescent nanoprobes for the detection of vitamin B12

Used luminescent nanoprobe	Technique	Linear range	LOD	Ref.
Mn^{2+}-doped ZnS QDs	Fluorometric	4.9–29.4 pM	1.15 ± 0.06 pM	This work
Graphene SAMs – C-dots	Fluorometric	4.98–33.8 nM	2.58 nM	6
Bombyx mori silk fibroin protein	Fluorometric	10–170 nM	20 nM	7
Thermally reduced C-dots	Fluorometric	1–12 μM	100 nM	8
N,S co-doped C-dots	Fluorometric	14.7–74 μM	5.8 μM	9
C-Dots	Fluorometric	0.3–15 mM	93 nM	10
C-Dots	Fluorometric	0.73–10.3 nM	81 nM	11
Boron doped C-dots	Fluorometric	0.20–30 μM	8.0 nM.	12
N,S co-doped C-dots	Fluorometric	0–114.6 μM	15.6 nM	13
N doped C-dots	Fluorometric	1 nM to 20 μM	210 pM	14
CdTe QDs	Fluorometric	0.73–10.3 nM	11 nM	15
Cu-nanoclusters	Fluorometric	4–28 μM	3.3 nM	16

amount of VB12 following quenching in their luminescence at 587 nm. Notably, the Stern–Volmer (SV) plot is inferred to demonstrate the quenching process of the emission intensity of Mn^{2+}-doped ZnS QDs following VB12 addition. Fig. 2D depicts the Stern–Volmer plot of the ratio of emission intensity (I_o/I) of the Mn^{2+}-doped ZnS QDs against the VB12 concentration. According to the Stern–Volmer equation,

$$\frac{I_o}{I} = 1 + K_{SV}[\mathrm{VB12}] \quad (1)$$

where I_o and I represent the emission intensities of the Mn^{2+}-doped ZnS QDs in the absence and in the presence of VB12.[6–16] Linearity was found in the range 4.9–29.4 pM with a correlation coefficient (R^2) of 0.99. The value of K_{SV} was calculated to be 5.2×10^{10} M^{-1}. The high SV constant value suggests that there might be an interaction between the Mn^{2+}-doped ZnS QDs and VB12.

Essentially, the selectivity of the Mn^{2+}-doped ZnS QDs towards the sensing of VB12 was tested in the presence of interfering amino acids (such as tryptophan, lysine, arginine, and glycine), metal ions (such as Mg^{2+}, Ca^{2+}, K^+, and Na^+), and protein (such as bovine serum albumin). Noticeably, no substantial variation in the luminescence intensity (I_{587}) of Mn^{2+}-doped ZnS QDs, upon addition of the above-mentioned interfering amino acids, metal ions, and protein, was observed (Fig. 2E). This clearly indicated the high selectivity of the Mn^{2+}-doped ZnS QDs towards the detection of VB12 in the presence of the aforementioned interfering amino acids, metal ions and protein. Thus the presented strategy could be useful for future biosensing purposes.

The mechanism behind the quenching of the emission of Mn^{2+}-doped ZnS QDs following the addition of VB12 can be explained as being primarily based on the FRET between Mn^{2+}-doped ZnS QDs and VB12. As is clear from Fig. 2F, there is an integral overlap of the emission spectrum of Mn^{2+}-doped ZnS QDs and the UV-vis absorbance spectrum of VB12. This clearly indicated the possibility of non-radiative energy transfer like FRET from Mn^{2+}-doped ZnS QDs to VB12; where Mn^{2+}-doped ZnS QDs and VB12 act as donor and acceptor, respectively. On the other hand, the absorption spectrum of Mn^{2+}-doped ZnS QDs (with $\lambda_{ex} = 320$ nm) did not coincide with the absorption spectrum of VB12 (Fig. S3, ESI†). This ruled out the possibility of the direct extinction of the acceptor VB12 and also supported the possibility of FRET from Mn^{2+}-doped ZnS QD to VB12. The details of the calculation of FRET distance and energy transfer efficiency are described in the ESI.†[24–28] In brief, the Förster distance R_o, which is the distance at which FRET is 50% efficient, is calculated using the following equation:

$$R_o^6 = 8.8 \times 10^{-25}\kappa^2\eta^{-4}\phi J(\lambda) \quad (2)$$

where κ^2 is an orientation factor between the emission dipole of Mn^{2+}-doped ZnS QDs ($\kappa = 2/3$ for the current case) and the absorption dipole of VB12, η is the refractive index ($\eta = 1.33$) of the medium, ϕ is the quantum yield of Mn^{2+}-doped ZnS QDs in the absence of VB12 ($\phi = 0.07$), and $J(\lambda)$ is the overlap integral of the emission spectrum of Mn^{2+}-doped ZnS QDs and the absorption spectrum of VB12. $J(\lambda)$ is calculated using the formula:

$$J(\lambda) = \frac{\int \mathrm{FD}(\lambda)\varepsilon(\lambda)\lambda^4 \mathrm{d}\lambda}{\int \mathrm{FD}(\lambda)\mathrm{d}\lambda} \quad (3)$$

where FD(λ) is the corrected emission intensity of Mn^{2+}-doped ZnS QDs with the total intensity normalized to unity, and $\varepsilon(\lambda)$ is the extinction coefficient of VB12. According to eqn (2) and (3), the value of $J(\lambda)$ was found to be 2.2×10^{-14} M^{-1} cm^3. The Förster distance (R_0) was calculated to be 2.33 nm. Importantly, the energy transfer efficiency was calculated using the following equation:

$$E = 1 - \frac{F_{DA}}{F_D} \quad (4)$$

where F_{DA} is the emission intensity of Mn^{2+}-doped ZnS QDs in the presence of VB12 and F_D is the emission intensity of Mn^{2+}-doped ZnS QDs in the absence of VB12. The FRET efficiency was estimated to be 79.3%.

$$E = \frac{1}{1 + (r_o/R_o)^6} \quad (5)$$

where r_o is the distance between Mn^{2+}-doped ZnS QDs and VB12 and is estimated to be 1.86 nm.

These results confirmed that the observed quenching of the luminescence of Mn^{2+}-doped ZnS QDs, upon addition of VB12, occurred primarily due to the FRET process. Additionally, no

significant changes were noticed in the emission intensity of Mn^{2+}-doped ZnS QDs, after adjusting their pH to that of VB12-added Mn^{2+}-doped ZnS QDs. This clearly ruled out the possibility of a pH effect on luminescence quenching of Mn^{2+}-doped ZnS QDs following the addition of VB12 (Fig. S4, ESI†). In addition, when the dispersion of the VB12-added Mn^{2+}-doped ZnS QDs was centrifuged and the pellet was redispersed into the same amount of solvent, the pellet showed a quenched emission intensity at 587 similar to that before centrifugation (Fig. S5, ESI†). This confirmed that there may be a possibility of interaction of the various functionalities (such as amide, phosphate, –OH or –CN groups) of VB12 with the labile dangling metal or sulfide bonds present on the surface of the Mn^{2+}-doped ZnS QDs.[29] Further, the decrease ($\Delta\zeta = 17$ mV) in the zeta potential value of Mn^{2+}-doped ZnS QDs following the addition of VB12 confirmed the presence of electrostatic interaction between Mn^{2+}-doped ZnS QDs and VB12 (Fig. S6, ESI†). This clearly confirmed that the binding of VB12 to Mn^{2+}-doped ZnS QDs is due to their mutual electrostatic interaction. Thus, the mechanism of luminescence quenching of Mn^{2+}-doped ZnS QDs by VB12 could be expected to be a combination of primarily FRET and an additional effect based on their mutual electrostatic interactions. Fig. 2G elucidates the FRET from orange-emitting Mn^{2+}-doped ZnS QDs to VB12 (with a transfer efficiency of 79.3% and R_o of 2.33 nm) – which primarily helped to detect VB12 with an LOD of 1.15 ± 0.06 pM.

In conclusion, the highly sensitive detection of VB12, especially at a picomolar level, using orange-red emitting ligand-free Mn^{2+}-doped ZnS quantum dots is reported for the first time. The sensing was achieved following the quenching of the luminescence of Mn^{2+}-doped ZnS QDs against an increasing concentration of VB12. The Stern–Volmer constant was estimated to be 5.2×10^{10} M^{-1}. Importantly, the Mn^{2+}-doped ZnS QDs displayed high sensitivity towards VB12, with a LOD as low as 1.15 ± 0.06 pM (in the linear range of 4.9–29.4 pM), showing the highly sensitive detection of VB12, especially at a picomolar level, compared to earlier reported luminescent nanoprobes. The presented nanoprobe showed high selectivity in the presence of the above-mentioned interfering amino acids, metal ions, and proteins. A FRET mechanism is primarily proposed for the detection of VB12, where Mn^{2+}-doped ZnS QDs acted as a donor and VB12 acted as an acceptor in the FRET pair. The Förster distance (R_o) and Förster efficiency (E) were calculated to be 2.33 nm and 79.3%, respectively. Furthermore, the presented concept may well bring forward newer ideas for constructing QD-FRET-based sensors in the near future.

Conflicts of interest

There are no conflicts to declare.

Acknowledgements

S. B. thanks the Department of Science and Technology (DST/INSPIRE/04/2017/001910; IFA17-CH287), Govt. of India, for funding. We thank Debarati Dey for her help with experiments. Assistance from CIF, IIT Guwahati, Mihir Manna and Milan Mahadani is acknowledged. We greatly acknowledge Prof. Arun Chattopadhyay for providing his lab facilities and endless support, help, and guidance.

Notes and references

1 (*a*) E. Alphandery, S. Faure, O. Seksek, F. Guyot and I. Chebbi, *ACS Nano*, 2011, **5**, 6279; (*b*) P. Tomcik, C. E. Banks, T. J. Davies and R. G. Compton, *Anal. Chem.*, 2004, **76**, 161.
2 (*a*) A. Miller, M. Korem, R. Almog and Y. Galboiz, *J. Neurol. Sci.*, 2005, **233**, 93; (*b*) Z. Rzepka, M. Respondek, J. Rok, A. Beberok, K. Ó. Proinsias, D. Gryko and D. Wrześniok, *Int. J. Mol. Sci.*, 2018, **19**, 2845.
3 K. S. Lok, S. Z. A. Muttalib, P. P. F. Lee, Y. C. Kwok and N.-T. Nguyen, *Lab Chip*, 2012, **12**, 2353.
4 H. W. Baik and R. M. Russell, *Annu. Rev. Nutr.*, 1999, **19**, 357.
5 G. Tsiminis, E. P. Schartner, J. L. Brooks and M. R. Hutchinson, *Appl. Spectrosc. Rev.*, 2017, **52**, 439.
6 W. T. Weng, X. Sun, B. Liu and J. Shen, *J. Mater. Chem. C*, 2018, **6**, 4400.
7 S. Chakravarty, B. Gogoi, B. B. Mandal, N. Bhardwaj and N. S. Sarma, *Biosens. Bioelectron.*, 2018, **112**, 18.
8 J. Wang, J. Wei, S. Su and J. Qiu, *New J. Chem.*, 2015, **39**, 501.
9 P. Tiwari, N. Kaur, V. Sharma, H. Kang, J. Uddin and S. M. Mobin, *New J. Chem.*, 2019, **43**, 17058.
10 X. Y. Sun, M. J. Yuan, B. Liu and J. S. Shen, *RSC Adv.*, 2018, **8**, 19786.
11 M. Wang, Y. Liu, G. Ren, W. Wang, S. Wu and J. Shen, *Anal. Chim. Acta*, 2018, **1032**, 154.
12 Y. Jia, Y. Hu, Y. Li, Q. Zeng, X. Jiang and Z. Cheng, *Microchim. Acta*, 2019, **186**, 84.
13 Y. Li, Y. Jia, Q. Zeng, X. Jiang and Z. Cheng, *Spectrochim. Acta, Part A*, 2019, **211**, 178.
14 G. Kalaiyarasan and J. Joseph, *Microchim. Acta*, 2017, **184**, 3883.
15 E. Vaishnavi and R. Renganathan, *Spectrochim. Acta, Part A*, 2013, **115**, 603.
16 K. Shanmugaraj, T. Sasikumar and M. IIanchelian, *J. Anal. Test.*, 2018, **2**, 168.
17 N. Pradhan and X. Peng, *J. Am. Chem. Soc.*, 2007, **129**, 3339.
18 B. B. Srivastava, S. Jana, N. S. Karan, S. Paria, N. R. Jana, D. D. Sarma and N. Pradhan, *J. Phys. Chem. Lett.*, 2010, **1**, 1454.
19 S. Pramanik, S. Bhandari, S. Roy and A. Chattopadhyay, *J. Phys. Chem. Lett.*, 2015, **6**, 1270.
20 S. Pramanik, S. Roy, A. Mondal and S. Bhandari, *Chem. Commun.*, 2019, **55**, 4331.
21 S. M. Shet, M. Bisht, S. Pramanik, S. Roy, S. Kumar, S. K. Nataraj, D. Mondal and S. Bhandari, *Adv. Opt. Mater.*, 2020, 1902022.
22 S. Bhandari, S. Roy, S. Pramanik and A. Chattopadhyay, *Langmuir*, 2015, **31**, 551.
23 S. Bhandari, S. Roy, S. Pramanik and A. Chattopadhyay, *Langmuir*, 2019, **35**(45), 14399.
24 J. Shi, F. Tian, J. Lyu and M. Yang, *J. Mater. Chem. B*, 2015, **3**, 6989.

25 (*a*) I. L. Medintz, A. R. Clapp, H. Mattoussi, E. R. Goldman, B. Fisher and J. M. Mauro, *Nat. Mater.*, 2003, **2**, 630; (*b*) D. M. Willard and A. V. Orden, *Nat. Mater.*, 2003, **2**, 575; (*c*) N. Soleja, N. Agrawal, R. Nazir, M. Ahmad and M. Mohsin, *Biotech*, 2020, **10**, 87.

26 (*a*) M. C. D. Santos, W. R. Algar, I. L. Medintz and N. Hildebrandt, *TrAC, Trends Anal. Chem.*, 2020, 115819; (*b*) Q. Chen, A. Kiraz and X. Fan, *Lab Chip*, 2016, **16**, 353.

27 A. Jaiswal, P. Sanpui, A. Chattopadhyay and S. S. Ghosh, *Plasmonics*, 2011, **6**, 125.

28 P. Maity, T. Gayathri, S. P. Singh and H. N. Ghosh, *Chem.–Asian J.*, 2019, **14**, 1688.

29 K. S. Taraszka, E. Chen, T. Metzger and M. R. Chance, *Biochemistry*, 1991, **30**, 1222.

